Toward Device-free and User-independent Fall Detection Using Floor Vibration

KAISHUN WU, YANDAO HUANG, MINGHUI QIU, ZHENKAN PENG, and LU WANG, Shenzhen University, China

The inevitable aging trend of the world's population brings a lot of challenges to the health care for the elderly. For example, it is difficult to guarantee timely rescue for single-resided elders who fall at home. Under this circumstance, a reliable automatic fall detection machine is in great need for emergent rescue. However, the state-of-the-art fall detection systems are suffering from serious privacy concerns, having a high false alarm, or being cumbersome for users. In this article, we propose a device-free fall detection system, namely G-Fall, based on floor vibration collected by geophone sensors. We first decompose the falling mode and characterize it with time-dependent floor vibration features. By leveraging Hidden Markov Model (HMM), our system is able to detect the fall event precisely and achieve user-independent detection. It requires no training from the elderly but only an HMM template learned in advance through a small number of training samples. To reduce the false alarm rate, we propose a novel reconfirmation mechanism using Energy-of-Arrival (EoA) positioning to assist in detecting the human fall. Extensive experiments have been conducted on 24 human subjects. On average, G-Fall achieves a 95.74% detection precision on the anti-static floor and 97.36% on the concrete floor. Furthermore, with the assistance of EoA, the false alarm rate is reduced to nearly 0%.

CCS Concepts: • **Human-centered computing** → **Ubiquitous and mobile computing**; • **Hardware** → *Signal processing systems;*

Additional Key Words and Phrases: Fall detection, floor vibration, geophone, device-free, user-independent

ACM Reference format:
Kaishun Wu, Yandao Huang, Minghui Qiu, Zhenkan Peng, and Lu Wang. 2023. Toward Device-free and User-independent Fall Detection Using Floor Vibration. *ACM Trans. Sensor Netw.* 19, 1, Article 5 (February 2023), 20 pages.
https://doi.org/10.1145/3519302

1 INTRODUCTION

Worldwide, there were more than 703 million people aged over 65 years in 2019. By 2050, that number is projected to be more than double its size in 2017, hitting to around 1.5 billion [42]. For the seniors, fall is one of the most prevalent problems that they have to face daily. According to the World Health Organization, approximately 28–35% of adults aged 65 and older fall each year,

This research was supported in part by the China NSFC Grant (U2001207, 61872248, 61872246), Guangdong NSF 2017A030312008, Shenzhen Science and Technology Foundation (No. ZDSYS20190902092853047), the Project of DEGP (No. 2019KCXTD005, R2020A045), and the Guangdong "Pearl River Talent Recruitment Program" under Grant 2019ZT08X603.
Authors' address: K. Wu, Y. Huang, M. Qiu, Z. Peng, and L. Wang (corresponding author), CSSE, Shenzhen Univercity, Shenzhen City, Guangdong Province, China; emails: wu@szu.edu.cn, 2016040084@email.szu.edu.cn, qmhsam@gmail.com, 2016040084@email.szu.edu.cn.

1550-4859/2023/02-ART5 $15.00
https://doi.org/10.1145/3519302

increasing to 32–42% for those who aged over 70 [32]. The hazard of non-fatal falls commonly includes bruises, internal bleeding, and bone fractures. When it comes to a fatal one, the fall event will be the symbol of a man's death. Among all the fall injury events, about 60% of them happen at home [12]. Based on the statistics above, around 139 million people aged over 65 will fall at home at least once a year. Among them, a large number of elders who live alone cannot get medical treatment in time, and the prolonged lying on the ground may turn a non-fatal fall into a fatal one.

Numerous literature proposed fall detection machine using vision, **Inertial Measurement Units (IMUs)**, and radio frequency. However, none of these fulfills the requirement of being privacy protected, device free, user independent, and low false alarm. As a human fall will cause a huge impact on the floor, one way to detect a human fall is to analyze the floor vibration, but only few works can be mentioned. In Reference [25], the authors proposed an automatic fall detection machine by deploying an accelerometer on the floor. However, this system requires the assistance of an acoustic microphone at the same time. It only evaluates a mimicking human doll falling forward, and it is a data-based system that fails to work using other test samples.

To implement a reliable vibration-based fall detection system, we need to address the following challenges: (i) The floor vibration profiles induced by many other objects fall from a certain height are similar to human fall. How can we distinguish a risky fall event from others? (ii) It is impossible to let the elders fall on the floor to train a classification model as most systems do. Is there any way to realize a user-independent fall detection system by building a general template for all the elders? (iii) The demanding detection task also results in a high false alarm rate, making the system user-unfriendly. What could we do to reduce the false alarm rate without the intentional intervene by users?

To address the above challenges, we first introduce and analyze two typical falling mode: trip and slip. By comparing the waveform and spectrum of vibration signals induced by different events, we find out that a floor vibration profile of human fall has two special *transition states*. We characterize the **floor vibration events (FVEs)** based on the **Discrete Wavelet Transform (DWT)**, which provides a good tradeoff for signals between time and frequency domain and enables a good measurement of FVEs. Then we train a recognition template using **Hidden Markov Model (HMM)** with a small number of training samples (e.g., 50 fall samples in our baseline evaluation). Based on this recognition template, we are able to recognize the testing fall samples from untrained users.

However, some of the vibration events have a similar pattern of a human fall after applying DWT to the vibration signals and thus cause false alarms. For addressing the third challenge, we propose a reconfirmation mechanism in the assistance of **Energy-of-Arrival (EoA)** positioning to reduce the false alarm rate. EoA is an indoor positioning algorithm that calculates the ratio of received signal energy between each pair of sensors. In contrast to the **time difference of arrival (TDoA)** mechanism, which requires high temporal resolution provided by a high sampling rate, EoA requires no temporal information recorded by sensors but only the energy of arrival. This makes the EoA mechanism has a better performance especially when the sampling rate is low and the time estimation error is high.

We prototype two versions of G-Fall for two different types of floor, respectively. Three geophone sensors are deployed on the real-time fall detection system. Experiment results show that G-Fall can detect the human fall event effectively. G-Fall achieves 95.74% detection precision with a false alarm rate at 5.30% on the anti-static floor and 97.36% detection precision with a false alarm rate at 4.76% on the concrete floor. Furthermore, the false alarm rate is reduced to nearly 0% with the assistance of the EoA reconfirmation mechanism.

In summary, the main contribution of this article lies in the following aspects.

- To the best of our knowledge, G-Fall is the first work to realize a privacy-protected, device-free, user-independent, and low-false-alarm fall detection machine with geophone sensors.

- We propose a novel mechanism based on EoA that enables the system to achieve fine-grained indoor positioning without high sample frequency. The false alarm rate is reduced from 5.30% to nearly 0% using EoA.
- We design and implement the real-time automatic fall detection machine leveraging the floor vibration. Extensive experiments in a typical indoor scenario demonstrate its feasibility of fall detection, achieving high precision on the anti-static and concrete floor.

The remainder of this article is organized as follows. We first introduce the related work in Section 2. Then in Section 3, we analyze the vibration waveform and spectrum, followed by the description of design goals and three main modules of G-Fall in Section 4. We illustrate our methodology in Section 5. Section 6 explains the implementation details of G-Fall prototype. We provide evaluation results of G-Fall in Section 7. Finally, the discussion and conclusion are given in Sections 8 and 9, respectively.

2 RELATED WORK

Existing fall detection systems: Over the past decade, extensive human fall detection systems have been proposed, and the comprehensive survey are studied in References [31, 46, 48, 50]. Fall detection systems can be mainly categorized as following four classes: vision based, IMU based, RF based, and ambient sensor based.

Vision-based fall detection systems [5, 27, 41] can detect a falls event effectively after analyzing a series of images recorded by high-resolution cameras using complex activity recognition algorithms such as deep learning algorithms. Nonetheless, it lacks privacy concern; for example, it is impossible to employ a camera in the bathroom to detect a slip event. Moreover, the vision-based systems fail to work under dark environment and non-line-of-sight condition.

Numerous works utilized the embedded IMUs in the wearable device to detect a fall [22, 39, 44]. They can detect a fall event by monitoring and analyzing the reading changes of an accelerometer, gyroscope, and inclinometer. However, it is obtrusive and user unfriendly to carry a device, and elderly people always forget to wear the smartwatch.

Radio frequency is a good choice to realize device-free fall detection systems [1, 43, 45, 47]. They require no on-body device and bring no privacy issues, which makes the wireless radio the most promising and charming research trend to realize device-free fall detection systems. Nevertheless, the high false alarm rate long has been criticized, and the multipath effect of wireless signals make it difficult to work in a dynamic home environment. TL-Fall [52] attempts to mitigate the environmental influence on Wi-Fi using transfer learning but only achieving around 85% sensitivity and specificity.

As for ambient sensor-based system, audio [24] and floor vibration [25] are used to characterize a human fall. The audio-based systems need to sense the sound of everything in the surroundings and have poor resistance to noise, leading to a large proportion of false alarm. There are also many challenges in realizing a fall detection system using floor vibration. However, the vibration signals propagating through the floor suffer almost zero multipath effect. And the signals can retain well even in a dynamic and complex environment [10]. In this article, we propose a device-free, user-independent, and positioning-assisted fall detection system with only vibration sensors, which can accurately distinguish a human fall from daily living activities or other objects that fall from a certain height.

Vibration-based indoor positioning: Another important technique related to G-Fall is device-free indoor positioning. Occupants can be located with ambient sensors instead of carrying wearable devices. RF signals, acoustic, ultra-wideband, cameras, and so on, are used for indoor positioning. To reduce the multipath effect of RF signals and acoustic, Floc [10] suggested a vibration

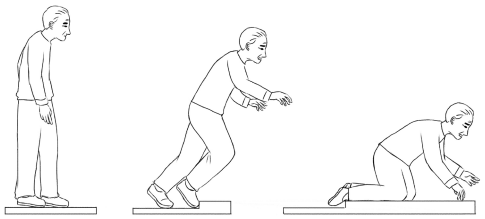

Fig. 1. Process of a trip.

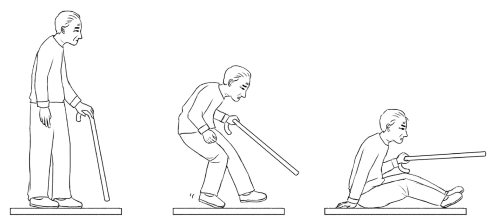

Fig. 2. Process of a slip.

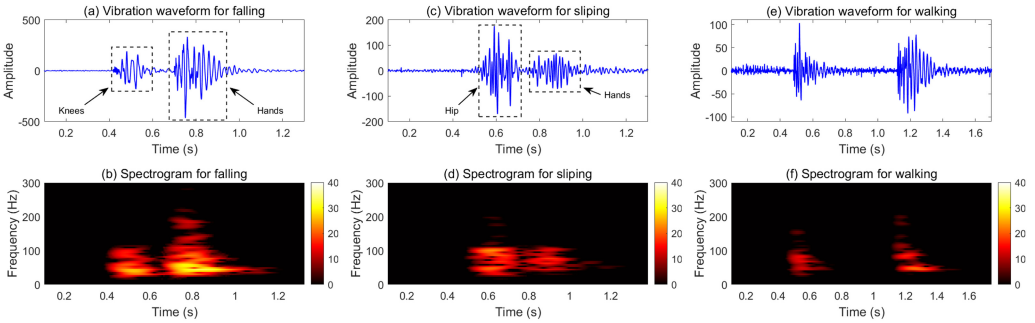

Fig. 3. Waveforms and spectrograms for body-induced vibration signals.

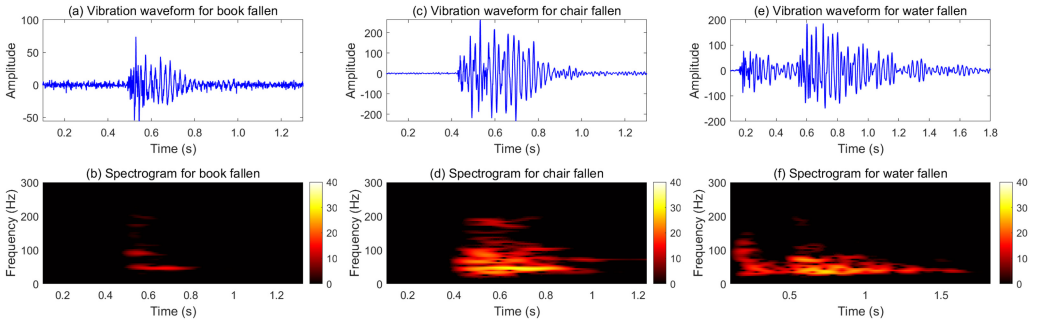

Fig. 4. Waveforms and spectrograms for object-induced vibration signals.

positioning methods with a SWIM algorithm to detect the footsteps. Reference [30] utilized the wavelet transform and TDoA to localize the vibration of footsteps. Pan et al. designed a hardware system called BOES [33] to collect footstep vibrations and track the occupants. However, these works required a high sampling rate to capture the precise value of TDoA. We propose an EoA mechanism to localize footsteps with the energy ratio between geophones in low frequency. We successfully reduce the false alarm rate to nearly 0% with EoA.

Vibration-based intelligent sensing: There have been many interesting vibration-based intelligent sensing system proposed in recent years [17]. FootprintID [36] utilizes footstep vibrations to identify occupants with an iterative transductive learning algorithm. Pan et al. [34] presented a method to monitor multiple occupant traffic by sensing the ambient structural vibration. The system achieves occupant traffic monitoring by acquiring signals from structural vibration sensors and analyzing their features. Bales et al. [3] used footsteps vibrations to classify gender. References [19, 20] used geophones to detect vibrations to monitor heartbeats when people are lying on a bed.

Some works [8, 9, 26, 35] use vibrations to localize finger tapping to realize text input. TouchPass [51] proposes a behavior-irrelevant on-touch user authentication scheme using the vibration of a smartphone. Vi-Liquid [16] utilizes the vibration from an iPhone to measure liquid viscosity and detects up to 30 kinds of unknown liquid. In contrast, G-Fall utilizes geophone sensors to collect floor vibration data and detect a human fall in the indoor environment.

3 PRELIMINARY STUDY

The key reasons that the elderly are involved in a fall event include the following: (i) Physical lesions incur uncoordinated walking or fainting, (ii) losing one's balance on a slippery floor such as in a bathroom, and (iii) falling over obstacles due to poor vision. Thus, we generally classified the falling mode as *trip* and *slip*, as shown in Figures 1 and 2. During the process of a trip, the knees usually hit the ground first, and then the hands on the ground provide support. In contrast, a slip leads to the hip landing first followed by the support of hands or elbows.

In a typical house environment, there are many FVEs, such as human footsteps and falling books, chairs, and bottles. Therefore, in this section, we first study the waveform and spectrum of the objects mentioned above.

Experimental setup: We set up the pilot test in a 6.0 × 8.0-m laboratory. Three geophones are respectively placed at three corners on the anti-static floor covering an area of 3.0 × 4.8 m, as shown in Figure 11. This area can be estimated as a typical area of a living room or bathroom. The sampling rate of G-Fall is set to be 1,190 Hz. For body-induced vibration, as shown in Figure 11, we collect the signals of trips and slips on the black cross area and the footsteps along the track with an interval of 60 cm. For object-induced vibration, we record the falling of a 400-ml bottle of water, a 400-page book, and a 2.5-kg chair. The bottle and book fall from a 50-cm-high desk.

Body-induced vibration: The waveform and spectrum of trip and slip are shown in Figure 3(a)–(d), where high-energy frequency components are colored in red. During a trip, the human body has a forward trend. In phase one, the knee is centered on the foot and uses the length of the calf as the radius to make the circular motion. But in phase two, the remaining parts of the body make the circular motion centered on landed knees, which results in a more considerable angular velocity when the hands are landing. This process is represented as a waveform of relatively low amplitude followed by a higher one in the time domain. As for a slip, in reverse, most of the falling force is neutralized when the hip is landing. The support hands suffer smaller force then.

There is a slight difference between a trip and slip, but they both comprise two obvious *transition states* on account that different part of the body contacts the floor in sequence. Because two parts of the body impact the floor one after another at a very short interval, the spectrum energy shows a transition pattern of "high-low-high." Compared to that of a footstep in Figure 3(e) and (f), a human fall has a longer duration, a shorter transition interval, and higher energy.

Object-induced vibration: When it comes to an object-induced vibration event, from Figure 4(a) and (c), the waveforms for the book and chair seem to be more stable, unlike that of a fall, which has two obvious *transition states*. This is because the rebound height of the chair is relatively low and even nonexistent for a book. As for the bottle, after the rebound, it tends to roll on the floor, resulting in longer vibration signals.

Summary of observations: From the analysis above, we have two observations: (i) the vibration signals of a fall event comprise two unique *transition states*, which is distinct from other events; and (ii) a fall event, compared to a walk event that is the main vibration source in daily life, has larger amplitude and longer duration. These two observations provide us with a hint to extract energy features and leverage the HMM to detect a human fall (see more details in Section 5).

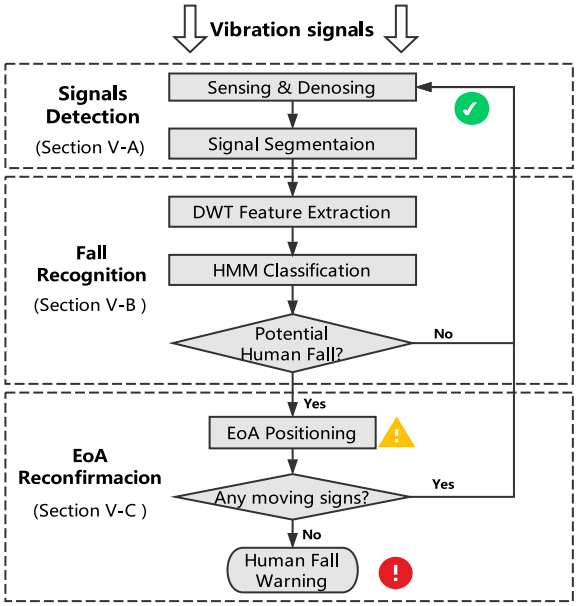

Fig. 5. System overview of G-Fall.

4 SYSTEM OVERVIEW

4.1 Design Goals

G-Fall is designed to meet the following goals, which are the basic features if we want to put G-Fall into practical use.

4.1.1 User-independent. Traditional fall detection systems are data based and adopt machine learning algorithms that require the users to train their own falling models in advance. However, it is impossible for these data-based fall detection machines to collect the fall data from the elderly. Therefore, G-Fall needs to find a way to make sure it is a user-independent system for specific users.

4.1.2 High Detection Precision. Timely fall detection and warning is about saving lives, and, ideally, we do not want to miss the detection of each human fall event. Thus, we have to make sure the system provides high detection precision for human falls.

4.1.3 Low False Alarm. It will be user unfriendly and obtrusive for elderly people if they need to clear the alarm every time a false alarm occurs. People take hundreds of steps a day, and then and then tens of warning messages will be sent if the false alarm rate is about 10%. Thus, we have to find a suitable solution to reduce the false alarm to zero as much as possible.

4.2 System Overview

The system architecture of G-Fall comprises three major components to build a reliable automatic fall detection system. The following is the description of these components.

4.2.1 Signal Detection. G-Fall employs three geophone sensors to convert the vibration signals into digitalized electrical signals. Then the signals are denoised using a 20-Hz Butterworth high-pass filter and segmented using an energy-based dual-threshold mechanism.

4.2.2 Fall Detection. In the classification phase, G-Fall extracts the unique features through DWT based on the observation after the decomposition of a fall event in the preliminary study. Then, a HMM is applied to complete fall detection.

4.2.3 EoA Reconfirmation. To realize a low-false-alarm fall detection system, in G-Fall, we adopt a straightforward but effective idea that leverages the assistance of indoor positioning. We come up with a novel positioning algorithm, EoA, which achieves decimeter-scale positioning and reduces the false alarm rate to nearly 0%.

Figure 5 presents the workflow of G-Fall. In the detection phase, the system continues to sense vibration signals that break the dual threshold. When a vibration event is sensed, the collected signals will be denoised and segmented. Afterwards, G-Fall extracts the signal features using DWT and matches the pattern with the pre-trained HMM template in the database to judge whether a potential human fall occurs. If so, then the EoA reconfirmation module will be turned on, and the system will reconfirm the potential human fall with EoA mechanism by detecting the moving signs of a human. A warning message will be sent out for asking help ultimately if there are no signs of human movement in a certain time; otherwise, the system will regard the potential human fall as a false alarm and keep sensing again without warning.

5 METHODOLOGY

In this section, we illustrate the details of G-Fall in three major modules.

5.1 Signal Detection and Process

5.1.1 Sensing and Denosing. The geophone is designed as a device for converting ground mechanical vibration signals into electrical ones. Figure 8 demonstrates the geophones we adopt, a cylinder whose external diameter is 25 mm and the height is 30 mm. It is sufficient to detect a fall with one geophone sensor, but the EoA positioning algorithm we design requires at least three geophones. Human fall-induced vibration signals are realized in the low-frequencies domain (less than 300 Hz), and we sample them using Raspberry Pi with a sampling frequency of 1,190 Hz. We leverage a 20-Hz Butterworth high-pass filter to remove the noise caused by the direct current component.

5.1.2 Segmentation. We adopt an energy-based dual-threshold scheme to catch a fall event [10]. The energy levels are calculated as the sum of the square of received signals in a sliding window. The lower threshold is $\mu + \sigma$, which is sensitive to break. And the higher one is $\mu + 3\sigma$. The μ and σ are the mean and standard deviation of signal energy, respectively. When the upper threshold is exceeded, the lower threshold will be considered as the start point of the detected signals. Three sensor channels have the same predefined dual threshold. If any one of three channels first breaks the predefined dual threshold, then the start point will be defined based on that one and shared across all channels. As for the endpoint, we set it at 0.8 seconds after the start point, as the duration of a fall is usually around it. Note that when a potential fall event is detected, the upper threshold will be reset for sensitive detection of a footstep in EoA. We deploy three sensors in G-Fall, but only one channel with the highest energy level will be segmented for feature extraction and input HMM.

5.2 Fall Event Detection

5.2.1 Feature Extraction. We model the fall event by profiling the energy of each component in the frequency domain derived from Time-Frequency analysis tool—**Short-Time Fourier Transform (STFT)**. However, to extract frequencies at multiple resolutions with respect to various time scales, the most relevant signal processing tool is DWT. Comparing to STFT, the advantages

of DWT are [45] as follows: (i) DWT performs a nice tradeoff between time and frequency resolution, and it groups frequencies that differ by several orders of magnitude into a few levels so that it can characterize the whole fall event. (ii) DWT reduces the size of the input sample so that the system can operate in real time. We calculate the energies for eight levels using Daubechies wavelets (db4) in the order of 6 and extract a 100-dimensional feature vector.

5.2.2 Detection with HMM. Recall that the observation in Section 2, we can infer that a senior is probably falling when looking at the transition between two states. HMM is a suitable method to establish a state transition model using time-dependent features. HMM has been successfully applied in several recognition applications such as speech [40], handwriting, and gesture [2] recognition. It is based on the assumption of a Markov chain: The state of the next moment is determined only by the current state and does not depend on any state in the past. The probability from the current hidden state to the next hidden state is defined as *transition probability*, and the probability of obtaining each potential observed value based on the current state is called *emission probability*. Afterwards, an HMM can be established given an *initial state vector*. We get the final HMM model $\boldsymbol{\lambda = (A, B, \Pi)}$ by using a small number of fall samples to train the three parameters: transition probability matrix $\boldsymbol{A}$, emission probability matrix $\boldsymbol{B}$, and initial state vector $\boldsymbol{\Pi}$. Given an *observation sequence*, i.e., the vibration signals, HMM will output a likelihood estimation that can tell how likely the input is to be a human fall.

Specifically, we estimate the mean vector and covariance matrix corresponding to each state and the transition probability with the well-known Baum-Welch algorithm [49]. The elements of transition probability matrix are initialized as 0.5, and the initial state vector is initialized as [1, 0, 0, 0, 0, 0, 0]. The number of hidden states is empirically set to 7 by iterating through a different number of states from 2 to 10, and we select the optimal one based on the results from the leave-one-user-out cross-validation. Note that the hidden states in HMM are abstract parameters that do not relate to the body state directly.

5.3 EoA Reconfirmation with Energy-of-Arrival

5.3.1 Why EoA?. To eliminate the obtrusive false alarm, we propose a straightforward yet effective idea that we can reconfirm the existence of a risky fall event with the assistance of indoor positioning. When a risky fall event occurs, in an ordinary situation, the elderly lose their ability to make any further movement to a new location. Therefore, if a series of movement activities are captured using an indoor positioning algorithm after a potential fall event is detected, then we can intuitively consider it a false alarm and clear the warning automatically without the intervention of humans. This makes the system practical and user friendly. Note that detecting any vibration signals is not a necessary hint to clear the alarm, because the fallen elder might stay conscious and struggle in situ, causing vibration on the floor.

Previous works [10, 30] realized decimeter-scale indoor multilateration with three geophones using TDoA algorithm. Estimating accurate time difference is essential for good positioning performance when using TDoA [11], but this requires more complex hardware to provide high sample frequency and thus increase the computation overhead. Furthermore, the dispersion nature of floor vibration during propagation resulting in different frequency components of wave travel at different velocities [14, 38]. As a result, the estimated propagation velocity of vibration signals varies largely, making an unacceptable shift for located points when using TDoA.

Thus, we come up with a novel algorithm EoA, which can realize fine-grained positioning at a low sample rate without the estimation of the time difference and propagation velocity.

5.3.2 EoA Model and Principle. The key innovation of G-Fall lies in reducing false alarm rate to zero using EoA mechanism with low sample frequency. The illustration of a multilateration

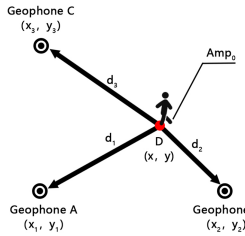

Fig. 6. An illustration of EoA positioning.

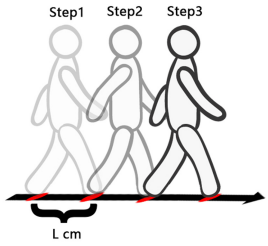

Fig. 7. An illustration of continuous walk for three steps.

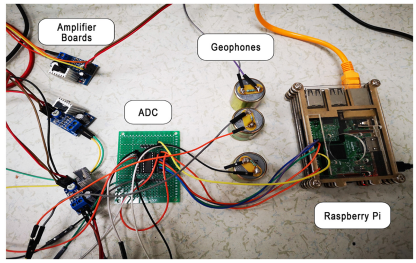

Fig. 8. Anti-static floor version prototype of G-Fall.

using three geophones is shown in Figure 6. Specifically, during the horizontal propagation of a footstep-induced vibration, the signals will suffer attenuation, and the model can be described as [7, 23]

$$Amp_2 = Amp_1\left(\frac{r_1}{r_2}\right)^n e^{-\alpha(r_2-r_1)}, \tag{1}$$

where Amp_1 and Amp_2 are the amplitude at propagation distance r_1 and r_2 from a vibration source, n and α are the damping coefficient, and the attenuation coefficient depends on the propagation media. The impact-induced vibration is dominated by the surface wave [3–5], and the damping coefficient n can be regarded as 0 [6]. Then, we can simplify the attenuation model as

$$Amp(d) = Amp_0 e^{-\alpha \times d}, \tag{2}$$

where Amp_0 is the initial amplitude of vibration source and d is the propagation distance. Now, the amplitudes of arrival for three geophones at certain distances d_1, d_2, d_3 respectively are

$$\begin{aligned} A(d_1) &= Amp_0 e^{-\alpha \times d_1} \\ B(d_2) &= Amp_0 e^{-\alpha \times d_2} \\ C(d_3) &= Amp_0 e^{-\alpha \times d_3}. \end{aligned} \tag{3}$$

We then can calculate the energy of arrival for the attenuated vibration signals from the reading of three geophone sensors. By dividing any pair of energy recorded by geophone, the initial amplitude of signals will be canceled out:

$$E_{AB} = \frac{A^2(d_1)}{B^2(d_2)} = \left(\frac{Amp_0 e^{-\alpha \times d_1}}{Amp_0 e^{-\alpha \times d_2}}\right)^2 = e^{-2\alpha \times (d_1 - d_2)}, \tag{4}$$

where E_{AB} is the ratio of energy of arrival from geophone A to that from geophone B.

Given signals from a coordinate-known point, we can calculate E_{AB}, d_1, and d_2. Then we can estimate an attenuation coefficient α of the floor from Equation (4). Afterwards, given any vibration signals generated from an unknown location, we have the following relationship based on the energy of arrival:

$$d_1 - d_2 = \frac{\ln E_{AB}}{-2\alpha} = 2a_1, \tag{5}$$

$$d_1 - d_3 = \frac{\ln E_{AC}}{-2\alpha} = 2a_2, \tag{6}$$

where a_1 and a_2 are the semi-major axis of two different hyperbolas, respectively.

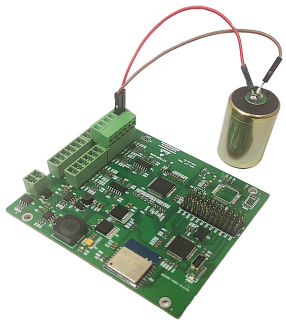

Fig. 9. Concrete floor version prototype of G-Fall.

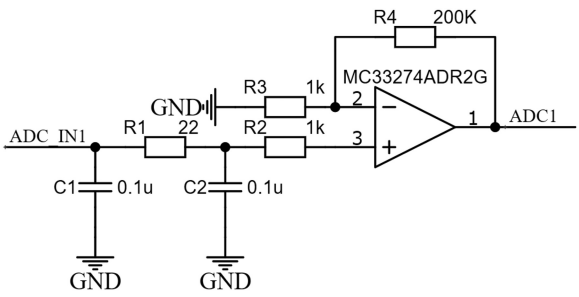

Fig. 10. The amplification circuit of the concrete floor version.

From Equation (5), we find that the unknown point *D(x,y)* is a moving point that the difference of the distances from two fixed points is a constant, which means the trajectory of *D(x,y)* is one side of a hyperbola. And the intersection of another hyperbola is the estimation of vibration source.

5.3.3 Detection of Moving Signs. To illustrate the basic idea, we depict a continuous walk of three steps with stride length of L cm in Figure 7. Given that the estimated coordinate of a fall position is $P_0(n_0, m_0)$ and that of next three steps is $P_1(n_1, m_1)$, $P_2(n_2, m_2)$, $P_3(n_3, m_3)$, respectively, we acquire a distance metric Dis to measure a movement,

$$Dis = \sum_{i=1}^{3} \sqrt{(n_i - n_0)^2 + (m_i - m_0)^2}. \tag{7}$$

The stride length varies from 40 to 80 cm for elderly subjects aged over 60 [18]. Assuming the 80% estimation error of EoA is below E cm, we can easily define a threshold. The threshold is hard to reach if a potential fall event is detected and the fallen subject struggles in situ. G-Fall regards the potential fall event as a real and fatal one and sends a warning message if the threshold is not exceeded in a pre-set time. But once it is overpassed, we consider whether further movement of a human occurs, and the potential fall event is a false alarm.

6 IMPLEMENTATION

As shown in Figure 8, we implement the first version prototype, which is suitable for an anti-static floor with a Raspberry Pi 3 controller and a 10-bit **Analog to Digital Converter (ADC)** MCP3008. Three geophones (LGT-4.5) [4] are connected to the controller through a cable for the collection of vibration signals. The received vibration signals are amplified by TDA2030A amplifier. We used the setClockDivider SPI of BCM2835 Library [28] with C to fix the sampling rate as 1,190 Hz. To set up a real-time system, we transmitted signals to a conventional desktop computer by a PL2303 USB to Transistor-transistor logic Converter Adapter Module via WiringPi Library with C. The data are then analyzed in the MATLAB platform. The recognition result of each vibration sample will be reported immediately without noticeable latency.

However, the first version prototype cannot apply to the concrete floor. The detection sensitivity is not high enough, and the signal-to-noise ratio is extremely low even if we cause a huge impact around the geophone sensor. Thus, we design a second version prototype for the concrete floor scenario. The PCB is equipped with an STM32L476RGT6 **microcontroller unit (MCU)**. This MCU is an ultra-low-power microcontroller based on the high-performance Arm Cortex-M4 32-bit RISC core operating at a frequency of up to 80 MHz. The analog vibration signals are converted to digital

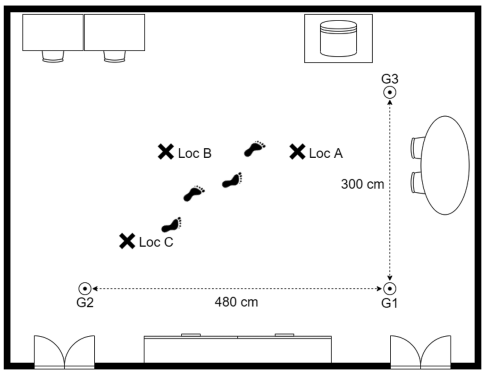

Fig. 11. A 8.0 × 6.0 m lab room with an anti-static floor.

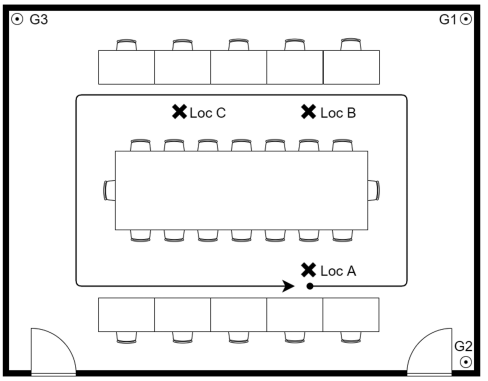

Fig. 12. A 8.5∗6.6 m meeting room with a concrete floor.

signals by the 16-bit ADC AD7606. The sampling rate is 3 kHz for each channel. The amplification circuit design is shown in Figure 10. The PCB needs a 12-V power source in exchange for higher amplification gain and sensitivity. We integrated the most typical yet cost-effective Wi-Fi MCU ESP8266 for signal transmission to the server end, which is responsible for further computation. A simple energy-based signal detection scheme is implemented to save power consumption. When there is no effective vibration signal, the PCB will stay in low-power mode. When the energy threshold is exceeded, it starts to transmit the vibration signals through Wi-Fi TCP protocol. The power consumption at transmission mode is around 1.5 W.

7 EVALUATION

This section will present experimental settings of G-Fall first, followed by the results for detecting a human fall event under different setting and verifying the effectiveness of EoA mechanism.

7.1 Experimental Setup

We evaluate our system in two scenarios. The first experiment environment is a typical 8 × 6 m laboratory with an anti-static floor. Three geophone sensors cover an area of 3×4.8 m as shown in Figure 11. There is no furniture blocking between the sensors. The second experiment environment is a 8.5 × 6.6-m meeting room with a concrete floor, as shown in Figure 12. Three geophones are deployed in the corner of the room. Some chairs and tables are in the middle of the room, blocking the sensors.

For the anti-static floor, we recruited 12 participants (2 of them are female) whose height, weight, and age are in the range of 156–182 cm, 48–68 kg, and 19–29, respectively. For the concrete floor, we recruit another 12 participants (3 of them are female) whose height, weight, and age are in the range of 160–185 cm, 43–81 kg, and 18–26, respectively. The height and weight of the participants is plotted in Figure 13. To form the main dataset, the participants are asked to perform the actions described in Table 1, each for 25 times. They are required to perform trips and slips depicted in Figures 1 and 2 as real as possible. Note that we do not collect slip samples on the concrete floor, because the **signal-noise-ratio (SNR)** is too low. In total, we collect 5,400 responses ((10 $actions$ + 2 $walks$×4 $steps$)×25 $times$×12 $subjects$) for the anti-static floor and 4,500 responses ((7 $actions$ + 2 $walks$ × 4 $steps$) × 25 $times$ × 12 $subjects$) for the concrete floor. We give a 2-minute warm-up period to the participants for practicing the required actions. As for objects, we drop a 400-ml bottle of water, a 400-page book, and a 2.5-kg chair, each for 25 times, respectively, generating

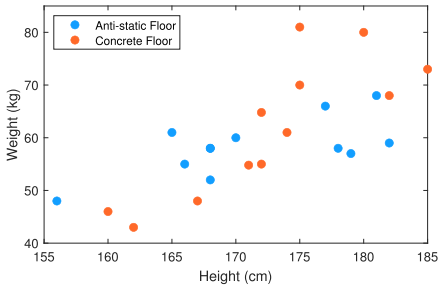

Fig. 13. The height and weight of participants.

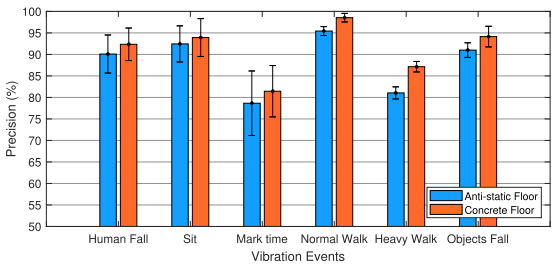

Fig. 14. The baseline performance of G-Fall with one person in the training set.

Table 1. Description of Actions for the Data Collection

Standard Fall	Loc.	Other Actions	Loc.
Trip forward	A	Sit	A
Trip forward	B	Mark time Heavily	A
Trip forward	C	Fall forward from a chair	A
Slip backward	A	Trip forward-Hold on a chair	A
Slip backward	B	Walk normally along the track	Track
Slip backward	C	Walk heavily along the track	Track

75 responses (25 $times \times 3$ $objects$). All the data are collected and saved for off-line analysis with G-Fall system running in real time. Each experiment is repeated 10 times to get the average results. Note that all the participants are required to wear protective gear when falling, and a cushion is also used when performing slips to protect their hip bones. The whole process of falling brings no harm to the subjects. All the experiments involving human subjects have been approved by the Institutional Review Board at our university.

Metrics: We introduce two metrics to analyze the performance of G-Fall, namely detection precision ($Precesion$) and false alarm rate (P_{fls}). The definitions are shown as follows. Note that other events refer to all the non-human fall events,

$$Precision = \frac{\#\ of\ truly\ classified\ samples}{\#\ of\ samples}, \tag{8}$$

$$P_{fls} = \frac{\#\ of\ wrongly\ detected\ fall}{\#\ of\ other\ events}. \tag{9}$$

7.2 Detection Accuracy

7.2.1 Baseline Performance. We first perform a baseline test for detecting fall events with only one person in the training set. Specifically, all the fall samples in location A of each participant are used to train the HMM in turn before testing with the rest of the samples. The detailed statistics are depicted in Figure 14. For the anti-static floor, with only one person in the training set, 495.45 of 550 human falls are correctly detected, yielding a precision of 90.08% with the false alarm rate at 12.30% on average. For the concrete floor, 253.96 of 275 trip samples are detected as human falls. The average precision and false alarm rate are 92.35% and 11.29%, respectively. We mark these results as the baseline performance of G-Fall.

We notice that the majority of false alarms are composed of "heavy actions" like marking time and walking heavily. However, the other results show that our system is relatively robust, that is,

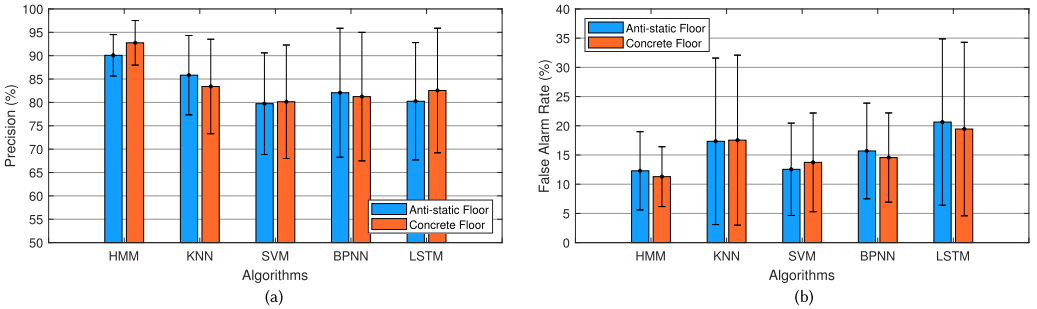

Fig. 15. Comparison of different classifiers with one person in the training set.

it will not register the normal daily activities as human falls. The uniqueness of a human fall is mainly denoted by the *transition state* mentioned in Section 3. The process of a human fall that we decompose has two parts of body contact with the floor, which can also be considered as two objects falling successively during a short time. This happens uncommonly and makes the human fall distinguishable from other events.

7.2.2 Comparison of Classification Algorithms. In this experiment, we compare the performance of HMM with other machine learning algorithms. Specifically, we select several classical classifier, namely, K-Nearest Neighbor [13], **Support Vector Machine (SVM)** [6], **Back Propagation Neural Network (BPNN)** [21], and **Long Short-Term Memory (LSTM)** [15]. For the first two classifiers, we calculate the Euclidean distance of samples (i.e., their DWT features) as the similarity metric. The kernel function of the SVM is the Radial Basis Function. BPNN and LSTM have one hidden layer with 128 hidden nodes. The learning rate is 0.05. The grid search optimization algorithm is applied to tune the hyper-parameters. The input features and the output are consistent with HMM model. The comparison regarding precision and false alarm rate are shown in Figure 15. The results show that HMM does present better performance when applying DWT, which extracts the time-dependent features from the vibration profile of a human fall. We can see that the LSTM network, which is also well known for characterizing sequential data, yield a poor detection performance. LSTM network surpasses HMM and then dominates the natural language processing field for decades, but it seems that the small dataset in our case results in an unacceptably inferior network.

7.2.3 Impact of Training Set Size. Since G-Fall characterizes the general fall event through a user-independent HMM template, we need to train the template as best as possible before practical use. Intuitively, the detection performance of our system can be improved by enlarging the training set size. To verify this hypothesis, we evaluate the performance by increasing the number of people in training set from 1 to 7. In Figure 16(a), we can see that the detection precision rises upward monotonically from 90.08% to 95.74% with an increase in the number of training people. The false alarm rate drop at the same time to the minimum of 5.30% with a seven-person-trained HMM. Overall, the system performance on the concrete floor is slightly better. The precision increases from 92.35% to 97.36%, while the false alarm rate decreases from 11.29% to 4.76% when the number of training people is equal to seven. This indicates that G-Fall will have a better performance if we increase the initial training sets by including more people's fall samples.

7.2.4 Impact of Different Locations. As a user-independent fall detection system, G-Fall should function properly and detect a human fall event at any location even though it depends on a template trained by the samples collected from a specific location. For example, if we build a template using the fall samples collected at location A, then the system should detect a fall at

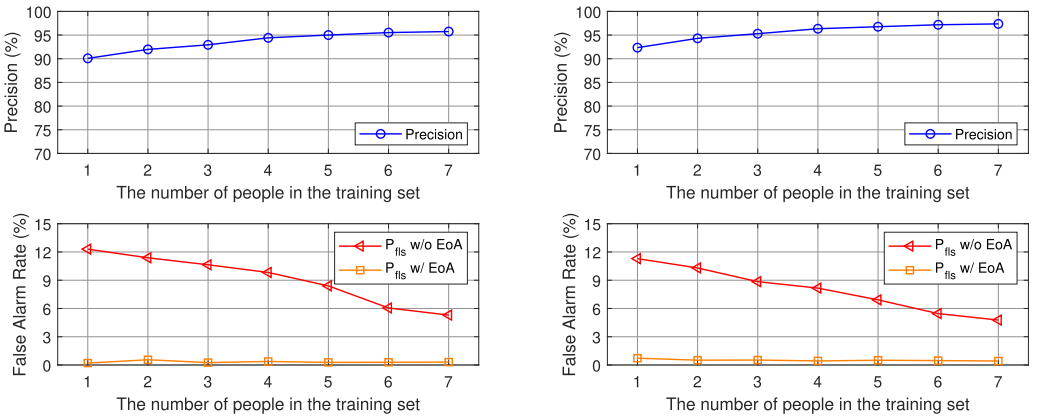

Fig. 16. Impact of training set size.

location B or C. To validate this hypothesis, we trained the HMM in turn with samples of each subject at location A and then tested it using the remaining fall samples collected at B and C. The results are shown in Figure 18, and, compared to the baseline, the precision suffers no degradation when testing with the samples from other locations. This verifies that G-Fall can detect human fall at anywhere even if we train the template with the human fall samples collected from only one specific location.

Figure 17(a)–(c) plots the vibration waveforms collected from different falling location and its corresponding DWT. From these figures, we observe that the DWT features that G-Fall extract follows similar energy transition pattern (i.e., "high-low-high"), even though the vibration waveforms vary from each other.

7.2.5 Impact of Non-standard Fall. We select two typical fall modes, trip and slip, as a standard to represent the majority of the fall event. However, there is a great variety of posture when users fall in practical. To study the impact when people perform non-standard falls, we ask our participants to fall from a 45-cm-heigh chair ($F_{chair@A}$) and fall with their hands held on the chair at the end of the fall ($H_{chair@A}$), each for 25 times. The collected non-standard samples are used to test a one-person-trained HMM. In Figure 18, we can see that the system performance suffers nearly no degradation when testing with non-standard fall samples. The result indicates that G-Fall can detect a certain falling pattern with HMM as classifier even when some posture variation of fall occurs. We think this is because the signals of floor vibration suffer less influence from complex human motions comparing to those fall detection systems that capture the human motions using accelerometer or gyroscope.

7.3 Effectiveness of Energy-of-Arrival

7.3.1 Accuracy of EoA. To realize positioning with TDoA and EoA, we first use three coordinate-known points to estimate the wave velocity v_0 and the attenuation coefficient α. Specifically, we induce vibration on known points 10 times and estimate the mean time delay Δt based on the received signals of two sensor. The distance difference from one known position to two sensor is Δd. Then v_0 is calculated as $\Delta t/\Delta d$, while α is calculated using Equation (4). The anti-static floor yields v_0 of 220 m/s and α of 0.2961, while the concrete floor gives v_0 of 262 m/s and α of 0.3722. Then we select the other six points as ground truth, estimating the coordinate for 20 times each using TDoA and EoA, respectively. Figure 19 shows the results of positioning performance for different sample

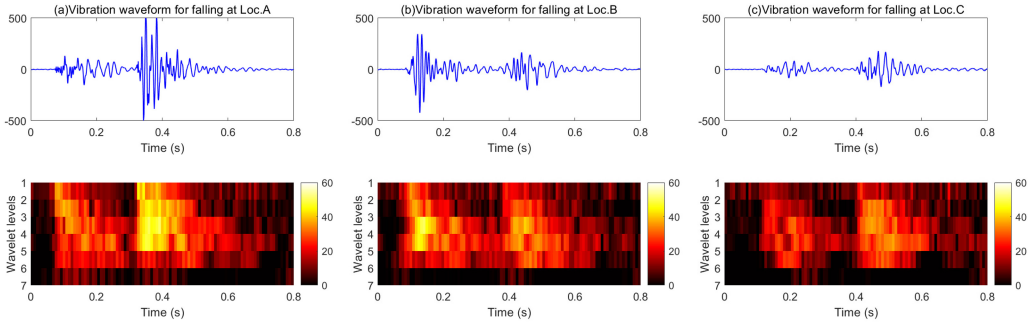

Fig. 17. DWT of time series for human fall at different location with regard to the same geophone.

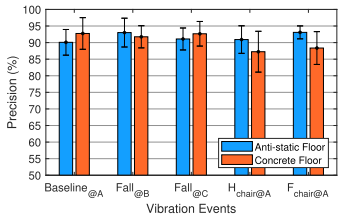

Fig. 18. Impact of different locations and nonstandard fall.

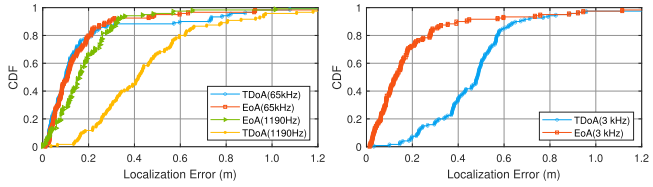

(a) Anti-static floor (b) Concrete floor

Fig. 19. The positioning error of TDoA and EoA with different sample rate.

rate and methods. EoA achieves nearly the same performance as TDoA with high sample rate at 65 kHz, and there is an 80% possibility where the positioning error goes below 20 cm. However, EoA outperforms TDoA when the sample rate drops to a low level (i.e., 1,190 Hz and 3 kHz).

This is because the estimation of time difference become inaccurate under the situation of low sample rate, leading to a considerable shift from the ground truth, while the estimation of energy requiring low temporal resolution and suffer no obvious degradation under the same situation. Moreover, the TDoA-based positioning system using geophones is based on the assumption that the wave propagates velocity is stable. However, in fact, during propagation, the velocity varies a lot in a different direction because of the dispersion nature [14, 38]. Therefore, the inaccurate estimation of time difference has a more significant impact on the positioning accuracy comparing to EoA whose assumption is that the attenuation coefficient of a specific media will not change.

7.3.2 After Reconfirmation with EoA. When a false alarm occurs, we assume that the elders will keep walking to clear the unsent alarm. Hence, we use the continuous four-step samples mentioned in the experimental setup to test the EoA reconfirmation module of G-Fall. So we can see from Figure 16 that when the EoA reconfirmation is turn on, the false alarm rate declined sharply to almost zero. However, indeed, the false alarm might still occur in some special case, but the results do verify the effectiveness of the EoA mechanism for reducing the false alarm rate.

7.4 Effective Sensing Range

In this experiment, we study the effective sensing range of G-Fall. Without loss of generality, we ask one of the participant whose height and weight is 180 cm and 65 kg to fall forward on the concrete floor. The distance between the falling position and sensor increases from 2 m to 10 m at a step size of 2 m. The participant falls forward 10 times at each position. We also collect the

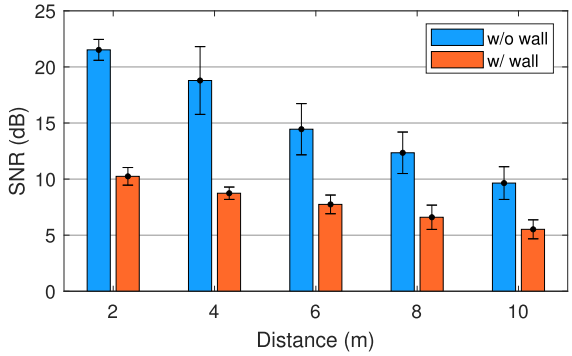

Fig. 20. The SNR of human fall vibration signals under different distances.

samples when there is a wall blocking in between. The SNR values of the collected raw vibration signals are shown in Figure 20. We can observe that the SNR decreases as the distance increases. In addition, the occlusion of the wall will reduce the SNR by about a half. With an effective sensing radius of 10 m, it is easy for G-Fall to cover the whole area of a typical family.

7.5 Through Wall Recognition

Through the previous experiment, we learned the effective sensing range of G-Fall by measuring the SNR. However, we do not give the exact recognition accuracy. Thus, in this experiment, we deploy our system in the corner of a new office room (denoted as R_C, concrete floor). We trained a seven-person HMM template model with samples collected in the meeting room (denoted as R_B, see Figure 12) but test with newly collected samples. The data collection setting is the same as the previous experiment, while the through-wall samples are collected from another office room (R_D) next to R_C. The newly collected fall samples from R_C and R_D have different SNR levels. The average recognition accuracy of all locations is 95.7%, which validates the cross-room and through-wall recognition ability of G-Fall.

7.6 Cross-domain Deployment

Finally, we would like to validate if G-Fall can deploy in the untrained environment with different floor types. In this experiment, we set the concrete floor as the source domain while the anti-static floor as the target domain. We first use the target domain samples to test on the seven-person HMM template trained on source domain samples without using any other techniques. The average accuracy degrades from 97.36% (intra-domain, see Figure 16(b)) to 80.01%. We then apply transfer learning techniques, namely transfer component analysis [37], to learn some transfer components that perverse data properties in a new subspace. However, the average accuracy unexpectedly drops by 5.85% to 75.06%. We speculate that the mapping function distorts the original features to some extent. Our attempt demonstrates that further exploration and improvement should be made for low-effort cross-domain deployment of G-Fall.

8 DISCUSSION

8.1 Dataset

One of the main limitations of this work is that the evaluation dataset only comprises young people's fall samples. In addition, we only consider two types of fall modes, namely trip and slip. The realistic fall is hard to be represented by only two modes. It is extremely difficult for researchers to collect elderly people's fall samples in the real world. Researchers need to recruit hundreds

of elderly volunteers for long-term data collection. Only a few test samples can be successfully collected in the end. Therefore, one future work will be how we can generate a larger dataset based on only a few realistic samples or how we can simulate the vibration signals regarding different falling postures. The generated or simulated data can then be used to train a more reliable model that detects elderly falls accurately.

8.2 Deploy across Different Floor Types

We evaluate our system on the anti-static floor and concrete floor. The anti-static floor provides good property in detecting vibration signals with high SNR. While on the concrete floor, we have to customize another device to capture the effective floor vibration. Our pilot study shows that collecting effective vibration signals on the carpet floor is infeasible. Most of the vibration is absorbed by the soft carpet, and the SNR is extremely low. For the future work, we plan to evaluate our system on more types of floor like wooden and tile floors. In addition, one might be thinking whether we can train a concrete floor HMM template and test with anti-static floor samples. Previous work [29] proposes to detect indoor occupants across different structures through footstep-induced floor vibration using transfer learning. We adopt the same transfer learning techniques in our dataset. However, no significant improvement has been achieved on cross-domain fall recognition. We think the domain adaption techniques will be helpful, but some other ways to use them should be tried in the future (e.g., transfer learning using a deep neural network).

8.3 Effective Detection Range

In our hardware setting, the effective detection range for the typical human fall is up to 10 m. It is sufficient for G-Fall to cover the area of a living room, bathroom, or even the whole house. We can enlarge the detection range with higher amplification. However, if the vibration source is closer to the sensor, then the amplitude of the received signals will also be higher. Then the low resolution of the low-cost ADC unit will bring another limitation, and we have to deploy a more expensive ADC unit.

8.4 Multi-person Sensing

G-Fall focuses mainly on detecting the fall of an elderly person who lives alone at home. If there is more than one person in the same sensing area simultaneously, then one should be able to help the fallen elder. However, what if the other person is a panicked young child when the elder falls? The child may cause floor vibrations at the same time when the elder falls, leading to a missed detection. Even if the fall is detected, the child may not know how to ask for help and move around the fallen elder, resulting in the alarm being cleared. For this case, we plan to apply blind source separation to separate mixed signals and then identify people by use of separated signals.

9 CONCLUSION

In this article, we propose G-Fall, a positioning-assisted, low-false-alarm, device-free, and user-independent automatic fall detection system for single-resided elders. G-Fall deploys three geophones on the cornersof a room to receive floor vibration signals. We analyze the floor vibration induced by the human fall and extract time-dependent features to distinguish a human fall from other events with a Hidden Markov Model. We prototype two versions of G-Fall, which can detect a fall event in real time on an anti-static floor and a concrete floor. The evaluation results demonstrate that G-Fall can accurately detect a human fall and has a high potential to be put into practical use.

REFERENCES

[1] Fadel Adib, Zachary Kabelac, and Dina Katabi. 2015. Multi-person localization via {RF} body reflections. In *Proceedings of the 12th USENIX Symposium on Networked Systems Design and Implementation (NSDI'15)*. 279–292.

[2] Jake K. Aggarwal and Michael S. Ryoo. 2011. Human activity analysis: A review. *ACM Comput. Surv.* 43, 3 (2011), 1–43.

[3] Dustin Bales, Pablo Tarazaga, Mary Kasarda, and Dhruv Batra. 2016. Gender classification using under floor vibration measurements. In *Dynamics of Coupled Structures, Vol. 4*. Springer, 377–383.

[4] Ltd. Baoding Longet Equipments Co. [n.d.]. LGT Seismic Geophone. Retrieved January 1, 2022 from http://www.longetequ.com/geophone/3.htm.

[5] Zhen-Peng Bian, Junhui Hou, Lap-Pui Chau, and Nadia Magnenat-Thalmann. 2014. Fall detection based on body part tracking using a depth camera. *IEEE J. Biomed. Health Inf.* 19, 2 (2014), 430–439.

[6] Chih-Chung Chang and Chih-Jen Lin. 2011. LIBSVM: A library for support vector machines. *ACM Trans. Intell. Syst. Technol.* 2, 3 (2011), 1–27.

[7] Aijun Chen, Feng Cheng, Di Wu, and Xianyuan Tang. 2019. Ground vibration propagation and attenuation of vibrating compaction. *J. Vibroeng.* 21, 5 (2019), 1342–1352.

[8] Wenqiang Chen, Lin Chen, Yandao Huang, Xinyu Zhang, Lu Wang, Rukhsana Ruby, and Kaishun Wu. 2019. Taprint: Secure text input for commodity smart wristbands. In *Proceedings of the 25th Annual International Conference on Mobile Computing and Networking*. 1–16.

[9] Wenqiang Chen, Maoning Guan, Yandao Huang, Lu Wang, Rukhsana Ruby, Wen Hu, and Kaishun Wu. 2018. Vitype: A cost efficient on-body typing system through vibration. In *Proceedings of the 15th Annual IEEE International Conference on Sensing, Communication, and Networking (SECON)*. IEEE, 1–9.

[10] Wenqiang Chen, Maoning Guan, Lu Wang, Rukhsana Ruby, and Kaishun Wu. 2017. FLoc: Device-free passive indoor localization in complex environments. In *Proceedings of the IEEE International Conference on Communications (ICC'17)*. IEEE, 1–6.

[11] P. T. Coverley and W. J. Staszewski. 2003. Impact damage location in composite structures using optimized sensor triangulation procedure. *Smart Mater. Struct.* 12, 5 (2003), 795.

[12] L. Day. 2003. *Falls in Older People: Risk Factors and Strategies for Prevention* S. R. Lord, C. Sherrington, and H. B. Menz (Eds.). Cambridge University Press, Cambridge, UK.

[13] Gongde Guo, Hui Wang, David Bell, Yaxin Bi, and Kieran Greer. 2003. KNN model-based approach in classification. In *OTM Confederated International Conferences: "On the Move to Meaningful Internet Systems."* Springer, 986–996.

[14] Joel B. Harley and José M. F. Moura. 2013. Sparse recovery of the multimodal and dispersive characteristics of lamb waves. *J. Acoust. Soc. Am.* 133, 5 (2013), 2732–2745.

[15] Sepp Hochreiter and Jürgen Schmidhuber. 1997. Long short-term memory. *Neural Comput.* 9, 8 (1997), 1735–1780.

[16] Yongzhi Huang, Kaixin Chen, Yandao Huang, Lu Wang, and Kaishun Wu. 2021. Vi-liquid: Unknown liquid identification with your smartphone vibration. In *Proceedings of the 27th Annual International Conference on Mobile Computing and Networking (MobiCom'21)*. Association for Computing Machinery, New York, NY, 174–187. https://doi.org/10.1145/3447993.3448621

[17] Yandao Huang and Kaishun Wu. 2020. Vibration-based pervasive computing and intelligent sensing. *CCF Trans. Perv. Comput. Interact.* 2, 4 (2020), 219–239.

[18] F. J. Imms and O. G. Edholm. 1981. Studies of gait and mobility in the elderly. *Age Ageing* 10, 3 (1981), 147–156.

[19] Zhenhua Jia, Musaab Alaziz, Xiang Chi, Richard E. Howard, Yanyong Zhang, Pei Zhang, Wade Trappe, Anand Sivasubramaniam, and Ning An. 2016. HB-phone: A bed-mounted geophone-based heartbeat monitoring system. In *Proceedings of the 15th ACM/IEEE International Conference on Information Processing in Sensor Networks (IPSN'16)*. IEEE, 1–12.

[20] Zhenhua Jia, Amelie Bonde, Sugang Li, Chenren Xu, Jingxian Wang, Yanyong Zhang, Richard E. Howard, and Pei Zhang. 2017. Monitoring a person's heart rate and respiratory rate on a shared bed using geophones. In *Proceedings of the 15th ACM Conference on Embedded Network Sensor Systems*. 1–14.

[21] Wen Jin, Zhao Jia Li, Luo Si Wei, and Han Zhen. 2000. The improvements of BP neural network learning algorithm. In *Proceedings of the 16th World Computer Congress and 5th International Conference on Signal Processing (WCC'00-ICSP'00)*, Vol. 3. IEEE, 1647–1649.

[22] Lih-Jen Kau and Chih-Sheng Chen. 2014. A smart phone-based pocket fall accident detection, positioning, and rescue system. *IEEE J. Biomed. Health Inf.* 19, 1 (2014), 44–56.

[23] Dong-Soo Kim and Jin-Sun Lee. 2000. Propagation and attenuation characteristics of various ground vibrations. *Soil Dynam. Earthq. Eng.* 19, 2 (2000), 115–126.

[24] Yun Li, K. C. Ho, and Mihail Popescu. 2012. A microphone array system for automatic fall detection. *IEEE Trans. Biomed. Eng.* 59, 5 (2012), 1291–1301.

[25] Dima Litvak, Israel Gannot, and Yaniv Zigel. 2008. Detection of falls at home using floor vibrations and sound. In *Proceedings of the IEEE 25th Convention of Electrical and Electronics Engineers in Israel*. IEEE, 514–518.

[26] Jian Liu, Yingying Chen, Marco Gruteser, and Yan Wang. 2017. Vibsense: Sensing touches on ubiquitous surfaces through vibration. In *Proceedings of the 14th Annual IEEE International Conference on Sensing, Communication, and Networking (SECON'17)*. IEEE, 1–9.

[27] Georgios Mastorakis and Dimitrios Makris. 2014. Fall detection system using Kinect's infrared sensor. *J. Real-Time Image Process.* 9, 4 (2014), 635–646.

[28] Mike McCauley. [n.d.]. C Library for Broadcom BCM 2835 as Used in Raspberry Pi. Retrieved January 1, 2022 from https://www.airspayce.com/mikem/bcm2835/group__spi.html.

[29] Mostafa Mirshekari, Jonathon Fagert, Shijia Pan, Pei Zhang, and Hae Young Noh. 2020. Step-level occupant detection across different structures through footstep-induced floor vibration using model transfer. *J. Eng. Mech.* 146, 3 (2020), 04019137.

[30] Mostafa Mirshekari, Shijia Pan, Pei Zhang, and Hae Young Noh. 2016. Characterizing wave propagation to improve indoor step-level person localization using floor vibration. In *Sensors and Smart Structures Technologies for Civil, Mechanical, and Aerospace Systems 2016*, Vol. 9803. International Society for Optics and Photonics, 980305.

[31] Nassim Mozaffari, Javad Rezazadeh, Reza Farahbakhsh, Samaneh Yazdani, and Kumbesan Sandrasegaran. 2019. Practical fall detection based on IoT technologies: A survey. *Internet Things* 8 (2019), 100124.

[32] World Health Organization. 2008. *WHO Global Report on Falls Prevention in Older Age*. World Health Organization, Ageing and Life Course Unit.

[33] Shijia Pan, Amelie Bonde, Jie Jing, Lin Zhang, Pei Zhang, and Hae Young Noh. 2014. Boes: Building occupancy estimation system using sparse ambient vibration monitoring. In *Sensors and Smart Structures Technologies for Civil, Mechanical, and Aerospace Systems 2014*, Vol. 9061. International Society for Optics and Photonics, 90611O.

[34] Shijia Pan, Mostafa Mirshekari, Pei Zhang, and Hae Young Noh. 2016. Occupant traffic estimation through structural vibration sensing. In *Sensors and Smart Structures Technologies for Civil, Mechanical, and Aerospace Systems 2016*, Vol. 9803. International Society for Optics and Photonics, 980306.

[35] Shijia Pan, Ceferino Gabriel Ramirez, Mostafa Mirshekari, Jonathon Fagert, Albert Jin Chung, Chih Chi Hu, John Paul Shen, Hae Young Noh, and Pei Zhang. 2017. Surfacevibe: Vibration-based tap & swipe tracking on ubiquitous surfaces. In *Proceedings of the 16th ACM/IEEE International Conference on Information Processing in Sensor Networks (IPSN'17)*. IEEE, 197–208.

[36] Shijia Pan, Tong Yu, Mostafa Mirshekari, Jonathon Fagert, Amelie Bonde, Ole J. Mengshoel, Hae Young Noh, and Pei Zhang. 2017. Footprintid: Indoor pedestrian identification through ambient structural vibration sensing. *Proc. ACM Interact. Mobile Wear. Ubiq. Technol.* 1, 3 (2017), 1–31.

[37] Sinno Jialin Pan, Ivor W. Tsang, James T. Kwok, and Qiang Yang. 2010. Domain adaptation via transfer component analysis. *IEEE Trans. Neural Netw.* 22, 2 (2010), 199–210.

[38] T. P. Philippidis and D. G. Aggelis. 2005. Experimental study of wave dispersion and attenuation in concrete. *Ultrasonics* 43, 7 (2005), 584–595.

[39] Paola Pierleoni, Alberto Belli, Lorenzo Palma, Marco Pellegrini, Luca Pernini, and Simone Valenti. 2015. A high reliability wearable device for elderly fall detection. *IEEE Sens. J.* 15, 8 (2015), 4544–4553.

[40] Lawrence Rabiner and Biing-Hwang Juang. 1993. Fundamentals of speech recognition. Prentice-Hall, Inc.

[41] Erik E. Stone and Marjorie Skubic. 2014. Fall detection in homes of older adults using the microsoft kinect. *IEEE J. Biomed. Health Inf.* 19, 1 (2014), 290–301.

[42] Department of Economic United Nations and Population Division Social Affairs. 2019. *World Population Ageing 2019: Highlights*. United Nations.

[43] Hao Wang, Daqing Zhang, Yasha Wang, Junyi Ma, Yuxiang Wang, and Shengjie Li. 2016. RT-Fall: A real-time and contactless fall detection system with commodity WiFi devices. *IEEE Trans. Mobile Comput.* 16, 2 (2016), 511–526.

[44] Jin Wang, Zhongqi Zhang, Bin Li, Sungyoung Lee, and R. Simon Sherratt. 2014. An enhanced fall detection system for elderly person monitoring using consumer home networks. *IEEE Trans. Cons. Electr.* 60, 1 (2014), 23–29.

[45] Wei Wang, Alex X. Liu, Muhammad Shahzad, Kang Ling, and Sanglu Lu. 2015. Understanding and modeling of wifi signal based human activity recognition. In *Proceedings of the 21st Annual International Conference on Mobile Computing and Networking*. 65–76.

[46] Xueyi Wang, Joshua Ellul, and George Azzopardi. 2020. Elderly fall detection systems: A literature survey. *Front. Robot. AI* 7 (2020), 71.

[47] Yuxi Wang, Kaishun Wu, and Lionel M. Ni. 2016. Wifall: Device-free fall detection by wireless networks. *IEEE Trans. Mobile Comput.* 16, 2 (2016), 581–594.

[48] Zhuo Wang, Vignesh Ramamoorthy, Udi Gal, and Allon Guez. 2020. Possible life saver: A review on human fall detection technology. *Robotics* 9, 3 (2020), 55.

[49] Lloyd R. Welch. 2003. Hidden markov models and the baum-welch algorithm. *IEEE Inf. Theory Soc. Newslett.* 53, 4 (2003), 10–13.

[50] Tao Xu, Yun Zhou, and Jing Zhu. 2018. New advances and challenges of fall detection systems: A survey. *Appl. Sci.* 8, 3 (2018), 418.

[51] Xiangyu Xu, Jiadi Yu, Yingying Chen, Qin Hua, Yanmin Zhu, Yi-Chao Chen, and Minglu Li. 2020. TouchPass: Towards behavior-irrelevant on-touch user authentication on smartphones leveraging vibrations. In *Proceedings of the 26th Annual International Conference on Mobile Computing and Networking*. 1–13.

[52] Lei Zhang, Zhirui Wang, and Liu Yang. 2019. Commercial Wi-Fi based fall detection with environment influence mitigation. In *Proceedings of the 16th Annual IEEE International Conference on Sensing, Communication, and Networking (SECON'19)*. IEEE, 1–9.

Received 15 August 2021; revised 5 February 2022; accepted 15 February 2022